6'-O-Caffeoylarbutin attenuates experimental hyperuricemia by regulating renal and intestinal urate transport, intestinal barrier integrity, and gut microbiota

XUEZHI YU[1], YANG ZHANG[1,2], KONCHUN SUN[1], RUI YANG[1,3], XINGDE LI[4], XIUZHEN CHEN[1], TIANTIAN LI[1], XIAOLEI YANG[1], MING LI[1], LU LIU[4], FEI LI[5] and BAOCHUN SHEN[1]

[1]School of Pharmaceutical Sciences and Yunnan Provincial Key Laboratory of Pharmacology for Natural Products, Kunming Medical University, Kunming, Yunnan 650500, P.R. China; [2]Department of Pharmacy, The Third People's Hospital of Yunnan Province, Kunming, Yunnan 650041, P.R. China; [3]School of Pharmacy, Chuxiong Medical College, Chuxiong, Yunnan 675005, P.R. China; [4]Department of Pharmacy, Kunming First People's Hospital, Kunming, Yunnan 650034, P.R. China; [5]School of Basic Medical Sciences, Kunming Medical University, Kunming, Yunnan 650500, P.R. China

Received March 19, 2026; Accepted July 16, 2026

DOI: 10.3892/mmr.2026.13992

Abstract. Hyperuricemia (HUA) is primarily attributed to insufficient uric acid (UA) excretion. 6'-O-Caffeoylarbutin (CA), the primary bioactive constituent of anti-gout herbal tea (Que Zui tea), has demonstrated potential urate-lowering effects; however, its underlying mechanisms require further elucidation. In the present study, a hypoxanthine (HX) and potassium oxonate (PO) induced hyperuricemia (HUA) mouse model was established to assess the effects of different doses of CA. Biochemical analyses, histopathological examination, western blotting and 16S rRNA gene sequencing were conducted to explore the underlying mechanisms. Notably, CA markedly reduced serum uric acid (SUA), serum creatinine (SCr) and blood urea nitrogen (BUN) levels and alleviated renal and intestinal histopathological damage. In the kidney, CA upregulated ATP-binding cassette sub-family G member 2 (ABCG2), and downregulated glucose transporter 9 (GLUT9) and urate transporter 1 expression (URAT1). In the intestine, CA increased ABCG2, PDZ domain containing 1 (PDZK1) and tight junction protein expression, while decreasing GLUT9, suggesting improved urate excretion and barrier integrity. 16S ribosomal RNA sequencing revealed that CA was associated with increased gut microbial diversity and reduced abundance of potentially harmful bacteria, including *Desulfovibrio*. Phylogenetic Investigation of Communities by Reconstruction of Unobserved States-based prediction suggested accompanying shifts in microbial functions related to transport and metabolism. In conclusion, these findings suggested that CA may exert beneficial effects on HUA involving regulation of renal and intestinal urate transport, improvement of intestinal barrier function and favorable modulation of gut microbiota. CA may therefore serve as a potential candidate for functional food development or therapeutic strategies against HUA.

Correspondence to: Professor Baochun Shen, School of Pharmaceutical Sciences and Yunnan Provincial Key Laboratory of Pharmacology for Natural Products, Kunming Medical University, 1168 Chunrong West Road, Chenggong, Yuhua, Kunming, Yunnan 650500, P.R. China
E-mail: shenbaochun@kmmu.edu.cn

Professor Fei Li, School of Basic Medical Sciences, Kunming Medical University, 1168 Chunrong West Road, Chenggong, Yuhua, Kunming, Yunnan 650500, P.R. China
E-mail: lifeii@kmmu.edu.cn

Abbreviations: ABCG2, ATP-binding cassette sub-family g member 2; BUN, blood urea nitrogen; GLUT9, glucose transporter 9; HUA, hyperuricemia; HX, hypoxanthine; IL-6, interleukin-6; PDZK1, pdz domain containing 1; PO, potassium oxonate; SCr, serum creatinine; SUA, serum uric acid; TNF-α, tumor necrosis factor-α; URAT1, urate transporter 1; ZO-1, zona occludens protein 1

Key words: 6'-O-Caffeoylarbutin; hyperuricemia, uric acid transporters, intestinal barrier, gut microbiota, multi-target mechanism

Introduction

Uric acid (UA) is primarily regulated by the liver, kidneys and intestinal tract to maintain systemic homeostasis. Disruption of this regulatory balance leads to elevated serum UA (SUA) levels (>420 μmol/l), resulting in hyperuricemia (HUA) (1). The global prevalence of HUA is steadily increasing; however, effective management strategies remain limited, thus imposing a growing burden on global public health systems (2). Although current pharmacological treatments effectively lower SUA levels, they typically target single mechanisms, such as xanthine oxidase (XOD) or urate transporter 1 expression (URAT1) inhibition. While combination therapy may enhance therapeutic outcomes, it also increases the risk of adverse effects (3,4). For example, febuxostat, a potent XOD inhibitor, has been associated with an increased risk of cardiovascular events (5-7) and previous survey data have indicated that 57.3% of patients treated with febuxostat and 59.4% of those treated with allopurinol experienced at least one notable

adverse effect (8). Similarly, benzbromarone, a uricosuric agent, is linked to hepatotoxicity (9) and the formation of UA nephrolithiasis (10). These limitations indicate the urgent need for safer and more effective multi-target therapies for HUA.

Of primary HUA cases, ~90% are attributed to insufficient UA excretion (11), which is primarily mediated by the kidneys (70%) and, to a lesser extent, by the intestines (30%) (12,13). UA excretion relies on various epithelial transporters, including URAT1, glucose transporter 9 (GLUT9) and ATP-binding cassette sub-family G member 2 (ABCG2) (14). Studies have shown that intestinal barrier dysfunction is closely associated with the development of HUA (15,16). Furthermore, chronic systemic inflammation, a hallmark of HUA, may arise from increased intestinal permeability, allowing microbial components such as lipopolysaccharide (LPS) to translocate into the bloodstream and trigger immune responses (17). UA-induced inflammation has been shown to disrupt intestinal epithelial integrity, further increasing gut permeability and exacerbating inflammation (18,19). Moreover, efficient intestinal excretion of UA requires a balanced gut microbiome (20); the gut microbiota can influence UA metabolism by modulating purine precursor production, uricolysis, metabolite balance and mucosal barrier integrity (21,22). Consequently, compared with therapies directed at a single target, such as suppression of UA production or modulation of renal urate transport, strategies acting on the kidney-gut axis may offer a more comprehensive approach to HUA management by facilitating extra-renal UA disposal, thereby partially relieving renal excretory burden, while also helping to preserve intestinal barrier integrity and microbial homeostasis, particularly in the context of impaired renal function (23). These findings suggest that investigating the kidney-gut-microbiota axis may offer more meaningful new perspectives and therapeutic strategies for the treatment of HUA.

6'-O-Caffeoylarbutin (CA), a prominent bioactive compound derived from the traditional anti-gout herbal tea (known as Que Zui tea), has recently gathered attention due to its diverse pharmacological properties. Research has predominantly focused on its anti-inflammatory and antioxidant effects (24,25). Notably, studies have demonstrated that CA exerts neuroprotective, hepatoprotective and nephroprotective effects (26-28). Additionally, CA has been shown to mitigate oxidative stress-induced tissue damage by modulating the nuclear factor erythroid 2-related factor 2 (Nrf2) signaling pathway (28) and to protect against acetaminophen-induced hepatotoxicity. The lipid-lowering and antithrombotic effects of CA have been validated in zebrafish models (29), demonstrating marked efficacy in improving lipid accumulation and oxidative stress in non-alcoholic fatty liver disease induced by a high-fat diet (30). In addition, the potent tyrosinase inhibitory effects of CA have been highlighted, suggesting its potential role in suppressing melanogenesis (31). Collectively, these findings suggest that CA exerts protective effects across multiple organ systems, particularly through anti-inflammatory and antioxidant mechanisms. However, it remains unclear as to whether CA influences the kidney-gut-microbiota axis to promote UA excretion and reduce its concentration, thereby ameliorating HUA. Therefore, it was hypothesized that CA may attenuate HUA through coordinated modulation of renal and intestinal urate transporters, restoration of intestinal barrier integrity and remodeling of gut microbiota composition, thereby promoting UA excretion and alleviating renal injury.

In the current study, a model of HUA was established in ICR mice and the mice were then administered CA to assess its effects on urate transporter expression in both the kidney and intestine, intestinal barrier function and gut microbiota composition. The aim of the present study was to uncover the multi-target mechanisms by which CA ameliorates HUA, with a particular focus on the kidney-gut-microbiota axis; this may provide new insights and potential therapeutic uses for CA.

Materials and methods

Materials and reagents. CA was isolated and purified from the leaf buds of Que Zui tea. Briefly, the dried Que Zui tea was crushed and extracted with 95% ethanol at a solid-to-liquid ratio of 1:10 (w/v). Ultrasonic extraction was performed three times at 40˚C (40 min each) using an ultrasonic frequency of 40 kHz. The combined extracts were then collected and concentrated to obtain the crude extract. Subsequently, 1.5 g crude extract was dissolved in 20 ml methanol, mixed thoroughly with 10 g silica gel and dried to remove the solvent. The resulting sample-silica gel mixture was subjected to chromatographic separation.

CA was further purified in semi-preparative mode using an LC-5520 high-performance liquid chromatography system (Beijing East & West Analytical Instruments Co., Ltd.) equipped with a homemade C18 column prepared in the School of Pharmaceutical Sciences and Yunnan Provincial Key Laboratory of Pharmacology for Natural Products (Kunming Medical University). Isocratic elution was performed using 30% methanol in water as the mobile phase at a flow rate of 1.0 ml/min. The CA-containing fractions were collected, concentrated to ~one-tenth of the original volume using a rotary evaporator, and maintained at 4˚C for 24 h. The resulting pale-yellow precipitate was then obtained by freeze-drying.

The purity of the isolated CA was determined by HPLC and was found to be 98.41% (Table SI). Briefly, the sample was dissolved in methanol, filtered through a 2.5-μm membrane and analyzed using an LC-2050C 3D HPLC (Shimadzu Corporation) system equipped with a Hypersil GOLD C18 column (Thermo Fisher Scientific, Inc.) at 25˚C. The mobile phase was 10% acetic acid-water/methanol (72:28, v/v), with a flow rate of 1.0 ml/min. The detailed chromatographic conditions are provided in Data S1 and the corresponding HPLC chromatogram is shown in Fig. S1. In addition, the chemical identity of CA was further confirmed by nuclear magnetic resonance (NMR) spectroscopy and its three-dimensional stereostructure was determined by single-crystal X-ray diffraction analysis. For NMR analysis, CA was dissolved in DMSO-d_6 and examined at 25˚C using a Bruker DRX-600M spectrometer (Bruker Corporation) at 600 MHz for ^{1}H-NMR and 150 MHz for ^{13}C-NMR. The experimental conditions for NMR analysis are described in Data S2, and the ^1H NMR and ^13C NMR spectra are presented in Figs. S2 and S3, respectively. For X-ray diffraction analysis, suitable CA single crystals were obtained from DMSO and data were collected at 150 (2) K using Cu Kα radiation (λ=1.54178 Å). The structure was solved using SHELXT (version 2025/1; https://www.shelx.uni-goettingen.de/), an integrated space-group and

crystal-structure determination program and refined using SHELXL (version 2025/1; https://www.shelx.uni-goettingen.de/), a crystal structure refinement program. The Flack parameter was 0.01(12). The detailed experimental procedures for single-crystal X-ray diffraction are provided in Data S3 and the corresponding results are shown in Figs. S4 and S5.

Establishment of a mouse model of HUA and drug administration. The present study was approved by the Animal Experiment Ethics Review Committee of Kunming Medical University (approval no. kmmu20240343) and performed in strict accordance with institutional guidelines for animal care and welfare, as well as the ARRIVE guidelines (https://arriveguidelines.org). A total of 36 specific-pathogen-free (SPF) male ICR mice (8 weeks old; 18-22 g) were obtained from SPF (Beijing) Biotechnology Co., Ltd. Male mice were used to reduce the potential variability associated with sex hormone fluctuations. The animals were housed under standard laboratory conditions at 22-26˚C and 40-60% humidity, with a 12-h light/dark cycle and free access to food and water.

After 1 week of acclimation, HUA was induced following a modified protocol based on a previous study (32). Briefly, with the exception of mice in the control group, all mice were administered hypoxanthine (HX; 500 mg/kg; Shanghai Titan Scientific Co., Ltd.) by oral gavage and potassium oxonate (PO; 300 mg/kg; Shanghai Titan Scientific Co., Ltd.) by intraperitoneal injection once daily for 14 consecutive days. The control mice received an equivalent volume of 0.5% sodium carboxymethyl cellulose. SUA levels were determined using an automated biochemical analyzer (Cobas c311; Roche Diagnostics GmbH) and successful model establishment was confirmed by an ~twofold increase in SUA levels compared with those in the normal control group. Mice were randomly assigned to six groups (n=6/group), as shown in Table I. The doses of CA (100, 200 and 300 mg/kg) were selected based on preliminary experiments, which indicated that this dose range was well tolerated, and exerted beneficial effects on SUA levels and renal injury in mice with HUA. A total of 1 h after HX and PO administration each day, mice in the CA treatment groups were orally administered CA at a volume of 0.1 ml/10 g body weight for 14 consecutive days. Body weight was recorded daily throughout the treatment period. Mice were fasted for 12 h before sample collection.

On the final experimental day, 1 h after the last administration, the mice were deeply anesthetized by intraperitoneal injection of sodium pentobarbital (120 mg/kg). Under deep anesthesia and prior to sacrifice, ~0.5 ml blood was collected from the retro-orbital venous sinus. The blood samples were left at room temperature for 1 h and then centrifuged at 1,000 x g for 10 min at 4˚C to obtain serum. Following blood collection, the mice were deeply anesthetized and sacrificed by cervical dislocation.

Histopathological examination [hematoxylin and eosin (H&E) staining. After the mice were sacrificed by cervical dislocation, the kidney and intestinal tissues were collected, rinsed with ice-cold phosphate-buffered saline until no visible blood remained, and then fixed in 4% paraformaldehyde at room temperature for 24 h. The tissues were then dehydrated through a graded ethanol series, cleared in xylene, infiltrated with molten paraffin, and embedded in paraffin blocks. Subsequently, the paraffin-embedded tissues were sectioned, deparaffinized in xylene and rehydrated through a graded ethanol series. The sections were stained with hematoxylin for 5 min at room temperature, differentiated in 1% acid alcohol for a few seconds, rinsed in running water for 5 min, and blued in ammonia water for 1 min. Subsequently, the sections were counterstained with eosin for 1-2 min at room temperature, dehydrated through graded ethanol, cleared in xylene, and mounted with neutral resin. Histological assessment was performed following hematoxylin and eosin (H&E) staining. Images of the stained slides were captured using an AU480 slide scanner (Beckman Coulter, Inc.) at x200 magnification. Renal histopathological injury was semi-quantitatively evaluated based on tubular epithelial degeneration, tubular dilation, epithelial desquamation and inflammatory cell infiltration. For each animal, five random non-overlapping fields in the renal cortex were analyzed. The injury scores were determined as follows: 0, no damage; 1, an injured area of 1-10%; 2, an injured area of 11-25%; 3, an injured area of 26-74%; and 4, an injured area of ≥75% (33). The mean score of five fields was calculated as the final renal injury score for each animal. Villus height and crypt depth in the small intestine were measured using ImageJ (version 1.8.0.345; National Institutes of Health). Blinding was not implemented during histopathological analysis, which represents a limitation of the current study.

Table I. Distribution of animal groups used in this study to assess health effects of CA.

Group	Gavage component
Control	0.5% CMC-Na
Model	HX (500 mg/kg) + PO (300 mg/kg) + 0.5% CMC-Na
BenZ	HX (500 mg/kg) + PO (300 mg/kg) + BenZ (10 mg/kg)
CA low	HX (500 mg/kg) + PO (300 mg/kg) + CA (100 mg/kg)
CA medium	HX (500 mg/kg) + PO (300 mg/kg) + CA (200 mg/kg)
CA high	HX (500 mg/kg) + PO (300 mg/kg) + CA (300 mg/kg)

CA, 6'-O-Caffeoylarbutin; CMC-Na, sodium carboxymethyl cellulose; HX, hypoxanthine; PO, potassium oxonate.

Assessment of intestinal permeability and inflammatory markers. Blood samples were allowed to clot at room temperature for 1 h, followed by centrifugation at 1,000 x g for 10 min at 4˚C to obtain serum. Serum levels of LPS (cat. no. A054-1-1; Nanjing Jiancheng Bioengineering Institute) and D-lactate (D-Lac; cat. no. A019-3-1; Nanjing Jiancheng Bioengineering Institute) were measured using commercial biochemical assay kits according to the manufacturer's instructions. Enzyme-linked immunosorbent assay kits were used to detect IL-6 (cat. no. KE10007; Wuhan Sanying Biotechnology) and TNF-α (cat. no. KE10002; Wuhan Sanying Biotechnology)

levels in serum and intestinal tissues according to the manufacturer's instructions.

Western blot analysis. Total protein was extracted from mouse intestinal and kidney tissues using RIPA lysis buffer (Beyotime Biotechnology) supplemented with 1% protease and phosphatase inhibitors. After homogenization and centrifugation, protein concentrations were determined using a bicinchoninic acid (BCA) protein assay kit (Beyotime Biotechnology). Absorbance was measured using a Plus 384 microplate reader (Molecular Devices, LLC), and a standard curve was generated according to the manufacturer's instructions to calculate the protein concentrations. Equal amounts of protein (30 μg per sample) was separated by SDS-PAGE on 8 or 10% gels, and was transferred onto 0.45-μm PVDF membranes using a wet transfer method. The membranes were blocked in 5% non-fat milk at room temperature for 2 h and then incubated overnight at 4˚C with the following primary antibodies: URAT1 (1:2,000; cat. no. 14937-1-AP), GLUT9 (1:800; cat. no. 26486-1-AP), ABCG2 (1:800; cat. no. 27286-1-AP), PDZ domain containing 1 (PDZK1; 1:1,000; cat. no. 10507-3-AP), zonula occludens 1 (ZO-1; 1:8,000; cat. no. 21773-1-AP), Claudin-1 (1:800; cat. no. 13050-1-AP), Occludin (1:8,000; cat. no. 27260-1-AP) and GAPDH (1:8,000; cat. no. 10494-1-AP; internal control; all from Wuhan Sanying Biotechnology). After washing, the membranes were incubated with a HRP-conjugated secondary antibody (1:8,000; cat. no. RGAR001; Wuhan Sanying Biotechnology) for 2 h at room temperature. Protein bands were visualized using an enhanced chemiluminescence detection kit (GLPBIO Technology LLC), and images were captured using a ChemiDoc™ XRS+ system (Bio-Rad Laboratories, Inc.). Densitometric analysis was performed using ImageJ software (version 1.54p; National Institutes of Health). The intensity of each target protein band was normalized to that of GAPDH from the same lane and relative protein expression levels were expressed as fold change vs. the control group. A total of five independent biological replicates were included in the western blot analysis for each group and the blot images presented in the figures are representative of these experiments. Blinding was not implemented during western blotting, which represents a limitation of the current study.

16S ribosomal RNA (rRNA) gene sequencing and analysis. To evaluate changes in gut microbial composition following CA intervention, cecal contents were collected from five randomly selected mice per group after euthanasia on the final day of the experiment. Microbial genomic DNA was extracted from cecal samples using the FastPure Stool DNA Isolation Kit (Shanghai Majorbio Bio-pharm Technology Co., Ltd.) according to the manufacturer's instructions. DNA integrity was assessed by 1% agarose gel electrophoresis, and DNA concentration and purity were measured using a NanoDrop 2000 spectrophotometer (Thermo Fisher Scientific, Inc.). The V3-V4 region of the bacterial 16S rRNA gene was amplified using primers 338F (5'-ACTCCTACGGGAGGCAGCAG-3') and 806R (5'-GGACTACHVGGGTWTCTAAT-3'). PCR was performed in a 20 μl reaction system containing 10 μl 2X Pro Taq, 0.8 μl each primer (5 μM), template DNA (10 ng/μl), and nuclease-free water to volume, using an ABI GeneAmp® 9700 thermal cycler (Thermo Fisher Scientific, Inc.). The cycling conditions were 95˚C for 3 min, followed by cycles of 95˚C for 30 sec, annealing for 30 sec and 72˚C for 45 sec, with a final extension at 72˚C for 10 min. Each sample was amplified in triplicate. PCR products were pooled, purified by 2% agarose gel recovery, and quantified using a Synergy HTX microplate reader (BioTek; Agilent Technologies, Inc.).

Purified amplicons were pooled in equimolar amounts. The concentration of the final pooled library was measured using a Qubit 4.0 Fluorometer (Thermo Fisher Scientific, Inc.), and the library was adjusted to a final concentration of 4 nM before loading onto the sequencing platform. The library was paired-end sequenced on an Illumina NextSeq 2000 PE300 platform (Illumina, Inc.) according to the standard protocols by Shanghai Majorbio Bio-Pharm Technology Co., Ltd. Raw sequencing data were processed using QIIME2 (34) with the DADA2 algorithm for denoising, and amplicon sequence variants were generated. α-diversity indices, including Chao1 and Shannon, were calculated using mothur software (version 1.30.2; http://www.mothur.org/wiki/Calculators) (35). Statistical significance between groups was assessed using the Wilcoxon rank-sum test. Principal coordinate analysis based on Bray-Curtis distance was used to assess β-diversity and PERMANOVA was employed to determine the significance of microbial community differences between groups. To evaluate the degree of microbial dysbiosis, the microbiome dysbiosis index was calculated based on markedly altered genera identified by the Wilcoxon rank-sum test, using the formula $\log_{10}$ [(total abundance of genera increased in the model group)/(total abundance of genera decreased in the model group)]. Functional profiles of the gut microbiota were predicted using Phylogenetic Investigation of Communities by Reconstruction of Unobserved States (PICRUSt2; version 2.5.2; http://huttenhower.sph.harvard.edu/galaxy) based on 16S rRNA gene sequences. ASV representative sequences were aligned to reference genomes for phylogenetic placement and gene family composition was inferred based on nearest sequenced relatives. The predicted gene families were subsequently annotated against the Kyoto Encyclopedia of Genes and Genomes (KEGG) Orthology database (https://www.genome.jp/kegg/ko.html) to identify KEGG Orthologs (KOs), and KO abundances were used for downstream functional analysis and visualization.

Statistical analysis. All data are presented as the mean ± standard deviation. Statistical analyses were performed using GraphPad Prism 10.0 (Dotmatics), unless otherwise specified. Prior to parametric analysis, data from each group were tested for normality using the Shapiro-Wilk test. Homogeneity of variances was assessed using the Brown-Forsythe test. For datasets satisfying the assumptions of normality and homogeneity of variance, differences among multiple groups were analyzed using ordinary one-way analysis of variance, followed by Dunnett's multiple-comparisons test with the model group as the reference group. For gut microbiota analysis, sequencing data processing, diversity analysis, taxonomic comparison, functional prediction and related figure generation were carried out using the Majorbio Cloud Platform (Majorbio Bio-Pharm Technology Co., Ltd.). Differences in microbiota-related data among groups were analyzed using the non-parametric Kruskal-Wallis H test, as appropriate. $P<0.05$ was considered to indicate a statistically significant difference.

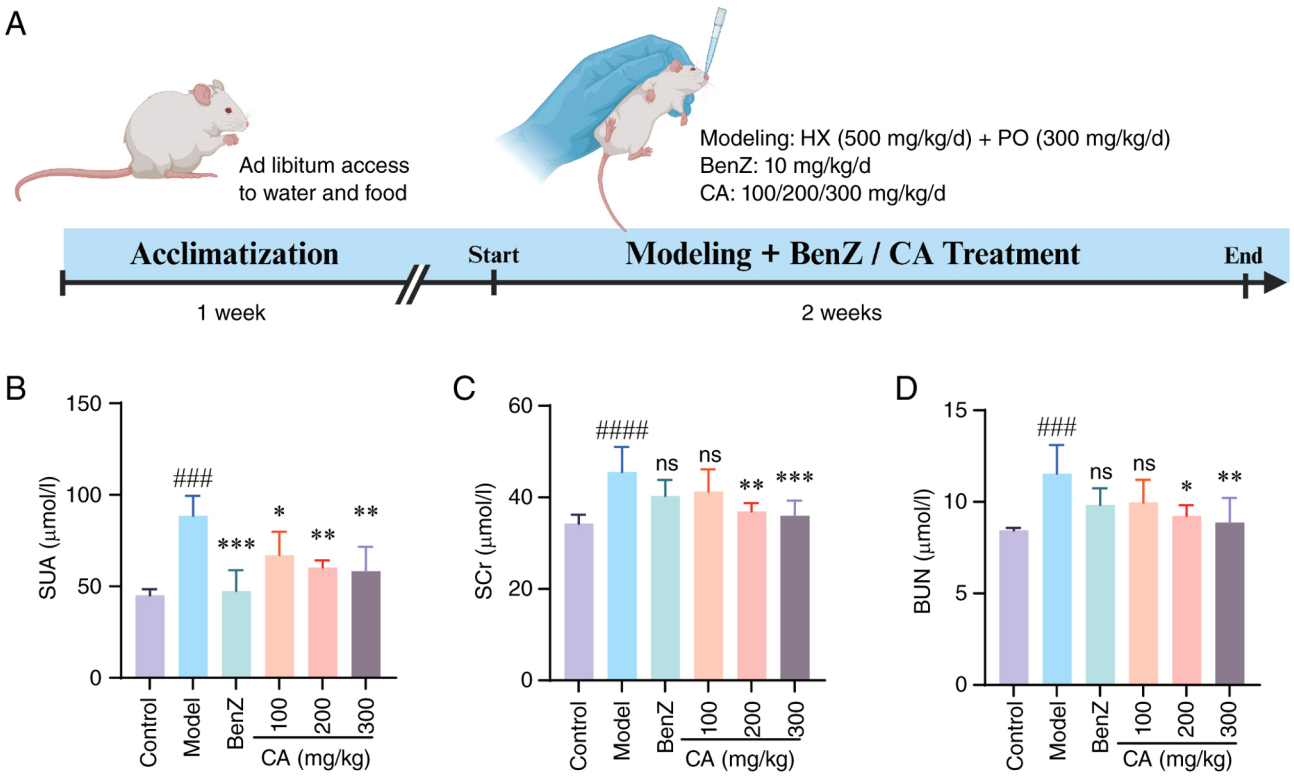

Figure 1. CA reduced SUA, SCr and BUN levels in hyperuicemia mice. (A) Schematic diagram of animal experiment design. (B) SUA levels. (C) SCr levels. (D) BUN levels. n=6. $^{###}$P<0.001, $^{####}$P<0.0001 vs. the control group *P<0.05, **P<0.01, ***P<0.001 vs. the model group. ns, no statistical significance; CA, 6'-O-Caffeoylarbutin; SUA, serum uric acid; SCr, serum creatinine; BUN, blood urea nitrogen.

Results

CA reduces SUA, SCr and BUN levels in mice with HUA. To evaluate the effect of CA on HUA, a mouse model of HUA was generated. Establishment of the HUA mouse model and administration of CA are shown in Fig. 1A. SUA is a key biochemical marker for evaluating HUA; compared with the control group, the model group exhibited a significant elevation in SUA levels (Fig. 1B), confirming successful model establishment. Following CA administration, all treatment groups exhibited a marked reduction in SUA concentrations relative to the model group. Similarly, SCr and BUN levels (Fig. 1C and D) were markedly decreased in CA-treated mice. These findings indicated that CA effectively mitigates HUA and demonstrates favorable renal safety at therapeutic concentrations.

Effects of CA on renal function in mice with HUA

CA alleviates renal injury in mice with HUA. Renal injury is a frequent complication of HUA. In the present study, gross anatomical examination revealed that HUA model mice had enlarged kidneys with pale, mottled surfaces and histopathological analysis using H&E staining further demonstrated tubular dilation, epithelial cell detachment and architectural disorganization in the model group (Fig. 2A). Concurrently, both the kidney-to-body ratio and the renal histopathology score were markedly increased in HUA model mice compared with the Control group (Fig. 2B and C), indicating marked renal swelling and histological injury. By contrast, CA-treated mice exhibited normalized kidney indices, dark red kidneys with smooth surfaces, and preserved renal histology without tubular dilation or epithelial shedding. Collectively, these data suggested that CA markedly attenuates HUA-induced renal injury.

CA modulates abnormal expression of renal UA transporters. The kidney is central to UA excretion; to determine whether CA modulates urate handling, the expression of key renal UA transporters was assessed by western blotting (Fig. 2D). As shown in Fig. 2E and F, the reabsorption transporters GLUT9 and URAT1 were markedly upregulated in the model group, whereas CA treatment markedly suppressed both GLUT9 and URAT1 expression. Conversely, expression of the urate efflux transporter ABCG2 was markedly reduced in the model group relative to the control group (Fig. 2G), and CA administration dose-dependently restored ABCG2 expression. These results suggested that CA promotes renal UA excretion by suppressing reabsorption and enhancing secretion, thereby restoring transporter homeostasis in HUA mice (Fig. 2H).

Effects of CA on intestinal function in mice with HUA

CA alleviates intestinal injury in mice with HUA. The intestine, a major extra-renal route for UA excretion, is highly susceptible to injury under hyperuricemic conditions, leading to functional impairment (36). To evaluate intestinal pathology, H&E staining of small intestinal tissues was performed. As shown in Fig. 3A, model group mice displayed severe mucosal damage, including widened villus gaps, villus loss and fragmentation. By contrast, CA group mice exhibited well-organized and intact villi without notable detachment

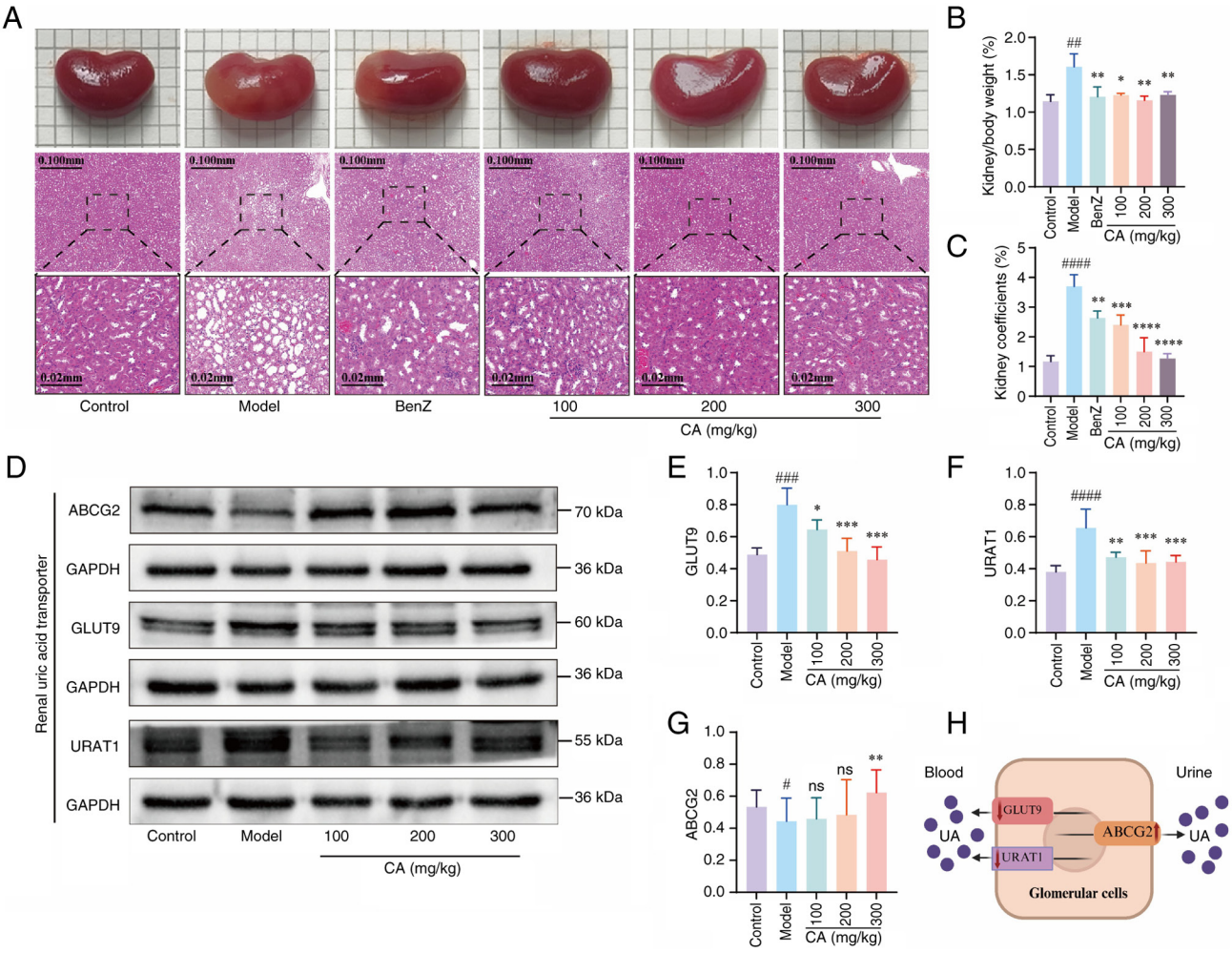

Figure 2. Effects of CA on renal function in HUA mice. (A) Representative kidney images and kidney sections stained with hematoxylin and eosin. Scale bar, 0.02 mm. (B) Kidney-to-body weight ratio. (C) Kidney organ coefficient. (D) Western blots of ABCG2, GLUT9 and URAT1. (E) Western blotting results of GLUT9. (F) Western blot results of URAT1. (G) Western blot results of ABCG2. (H) Schematic illustration of CA-mediated renal urate transport regulation. n=5. $^{\#}$P<0.05, $^{\#\#}$P<0.01, $^{\#\#\#}$P<0.001, $^{\#\#\#\#}$P<0.0001 vs. the control group. *P<0.05, **P<0.01, ***P<0.001, ****P<0.0001 vs. the model group. ns, no statistical significance; CA, 6'-O-Caffeoylarbutin; HUA, hyperuricemia; ABCG2, ATP-binding cassette sub-family g member 2; GLUT9, glucose transporter 9; URAT1, urate transporter 1.

or atrophy. Quantitative morphometry revealed markedly shortened villi and deepened crypts in the model group, reflecting hyperproliferative alterations (Fig. 3B). Notably, CA treatment restored villus length and partially normalized crypt depth (Fig. 3C). These findings indicated that CA effectively reversed HUA-induced intestinal damage and restores normal intestinal morphology.

CA alleviates intestinal inflammatory responses and decreases serum LPS, D-Lac and inflammatory cytokine levels. Inflammation is a major driver of intestinal injury in HUA (18). To evaluate the effects of CA on intestinal inflammatory responses and intestinal barrier function, the current study examined changes in inflammatory factors in intestinal tissue and related serum markers. As shown in Fig. 3D and E, compared with in the control group, the levels of TNF-α and IL-6 in intestinal tissue were markedly elevated in the model group, suggesting that HUA induced a marked intestinal inflammatory response. Following CA intervention, TNF-α and IL-6 levels in intestinal tissue were markedly decreased, indicating that CA can effectively alleviate HUA-associated intestinal inflammation. Further detection of serum LPS and D-Lac levels revealed that these were markedly elevated in the model group compared with those in the control group (Fig. 3F and G), suggesting increased intestinal permeability and impaired intestinal barrier function in HUA model mice. By contrast, after CA treatment, serum LPS and D-Lac levels were both markedly decreased, indicating that CA has a beneficial effect on intestinal barrier damage.

Concurrently, serum TNF-α and IL-6 levels in the model group were markedly higher than those in the control group (Fig. 3H and I), whereas these markers were markedly decreased following CA intervention. In summary, CA can alleviate systemic inflammatory responses in HUA model mice by suppressing intestinal inflammation and improving intestinal barrier function.

CA enhances the expression of intestinal tight junction proteins. To further assess intestinal barrier integrity, the expression levels of tight junction proteins ZO-1, occludin and claudin-1 were analyzed by western blotting (Fig. 4A). As shown in Fig. 4B and C, the expression levels of all

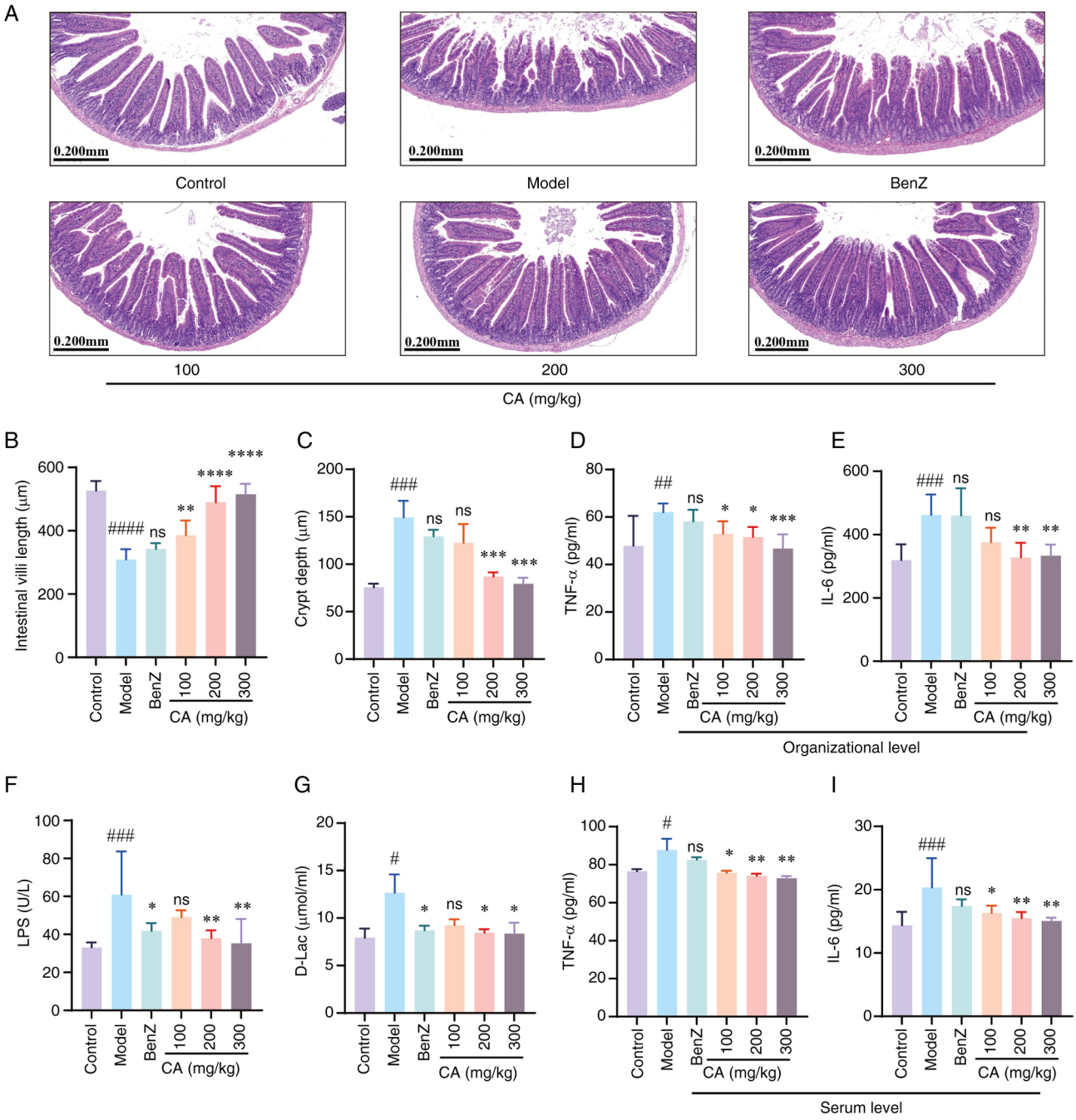

Figure 3. CA ameliorates intestinal injury. (A) Intestinal sections stained with hematoxylin and eosin. Scale bar, 0.200 mm. (B) Small intestinal villus length. (C) Small intestinal crypt depth. (D) TNF-α levels in small intestinal tissue. (E) IL-6 levels in small intestinal tissue. (F) Serum LPS levels. (G) Serum D-lactate levels. (H) Serum TNF-α levels. (I) Serum IL-6 levels. n=5. $^{\#}$P<0.05, $^{\#\#}$P<0.01, $^{\#\#\#}$P<0.001, $^{\#\#\#\#}$P<0.0001 vs. the control group. *P<0.05, **P<0.01, ***P<0.001, ****P<0.0001 vs. HUA Model group. ns, no statistical significance. CA, 6'-O-Caffeoylarbutin; TNF-α, tumor necrosis factor-α; IL-6, interleukin-6; LPS, lipopolysaccharide; HUA, hyperuricemia.

three proteins were markedly reduced in the model group compared with those in the control group, indicating impaired barrier function. By contrast, treatment with CA markedly restored their expression. These findings suggested that HUA compromises intestinal tight junctions, whereas CA preserves barrier integrity by upregulating tight junction protein expression (Fig. 4E).

CA modulates the expression of intestinal urate transporters. Intestinal urate transporters are essential for regulating UA absorption and excretion and their dysregulation contributes to HUA pathogenesis (37,38). Western blot analysis revealed a significant decrease in the intestinal expression of the UA efflux transporter ABCG2 and an increase in the reabsorption transporter GLUT9 in HUA model mice (Fig. 4G and H). By contrast, CA reversed these alterations. Expression of PDZK1, a scaffold protein that stabilizes ABCG2 at the apical membrane, was markedly reduced in the model group but restored in a dose-dependent manner following CA administration (Fig. 4I). Collectively, these results indicated that CA preserves intestinal UA excretion by upregulating ABCG2 and PDZK1, while downregulating GLUT9, thereby

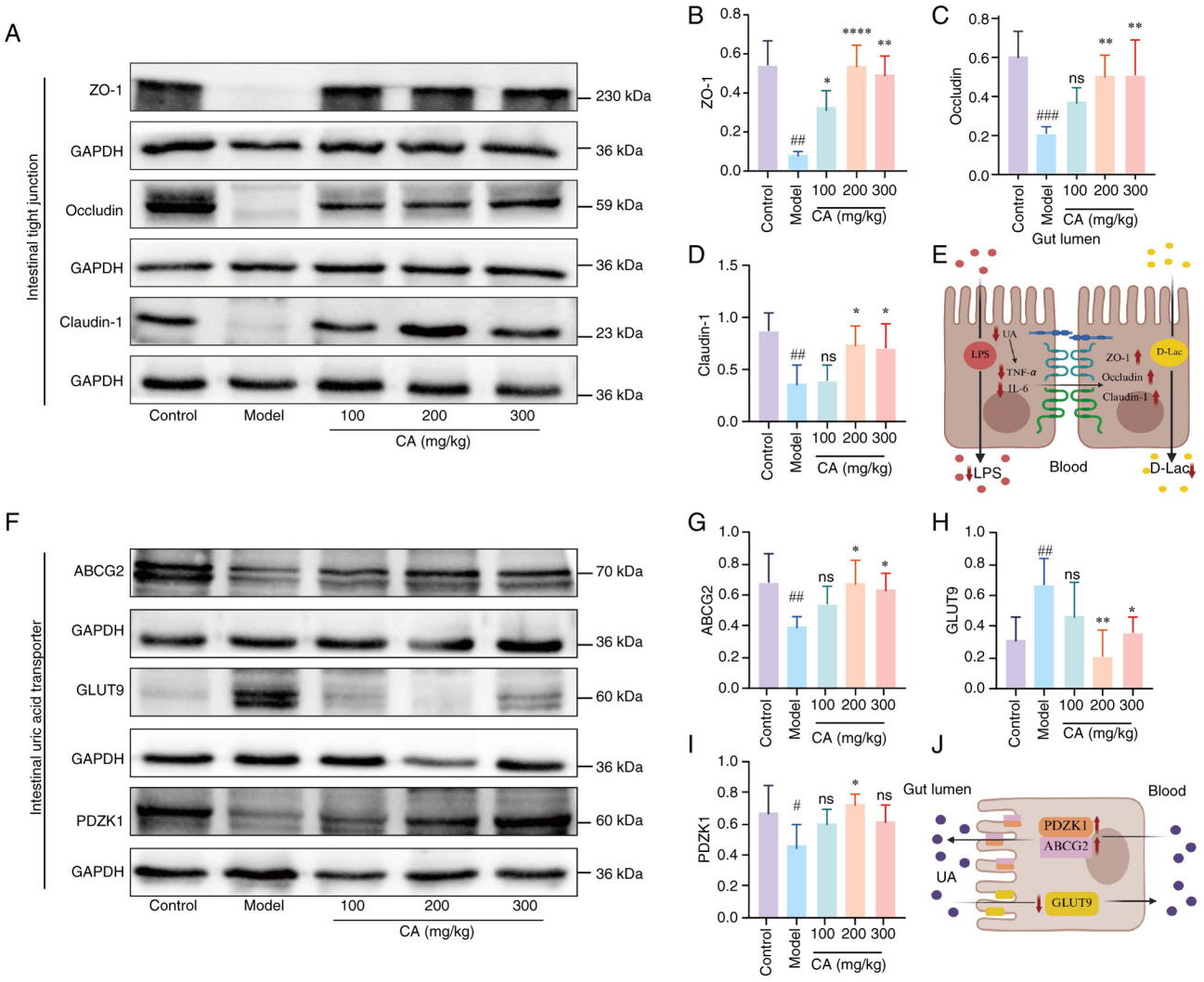

Figure 4. CA improves the expression of intestinal tight junction proteins and uric acid transporters. (A) Western blots of ZO-1, occludin and claudin-1. (B) Western blot results of ZO-1. (C) Western blot results of occludin. (D) Western blot results of claduin-1. (E) CA-mediated restoration of intestinal barrier integrity and reduction of intestinal permeability. (F) Western blots of ABCG2, GLUT9 and PDZK1. (G) Western blot results of ABCG2. (H) Western blot results of GLUT9. (I) Western blot results of PDZK1. (J) Schematic illustration of CA-mediated intestinal urate transport regulation. n=5. $^{\#}$P<0.05, $^{\#\#}$P<0.01, $^{\#\#\#}$P<0.001 vs. the control group. *P<0.05, **P<0.01, ****P<0.0001 vs. the model group. ns, no statistical significance. CA, 6'-O-Caffeoylarbutin; ZO-1, zona occludens protein 1; ABCG2, ATP-binding cassette sub-family g member 2; GLUT9, glucose transporter 9; PDZK1, pdz domain containing 1; URAT1, urate transporter 1.

contributing to its urate-lowering effects via the intestinal pathway (Fig. 4J).

CA ameliorates gut microbiota dysbiosis. The intestine harbors a dense microbial ecosystem that serves a pivotal role in metabolism, immune regulation and systemic homeostasis (39). Emerging evidence has implicated gut microbiota dysbiosis in the development of HUA and related metabolic disorders (40,41).

To examine whether CA modulates gut microbial composition, 16S rRNA gene sequencing was performed. β-diversity analysis revealed distinct clustering between the control and model groups, whereas the microbiota of CA-treated mice shifted toward the control profile (Fig. 5B). In addition, α-diversity indices (ace, chao, sobs and shannon) were markedly increased after CA administration (Fig. 5A), reflecting enhanced microbial richness and diversity. Furthermore, the microbiome dysbiosis index demonstrated that the CA group exhibited improved overall microbial health and mitigated dysbiosis (Fig. 5C).

The current study also analyzed the composition of the gut microbiota. At the phylum level, the intestinal microbiota of mice mainly composed of Firmicutes, Desulfobacterota, Bacteroidota, Verrucomicrobiota and Patescibacteria (Fig. 5D). In comparison with the control group, the model group exhibited structural changes, including a reduced Firmicutes ratio, and increased proportions of Desulfobacterota and Verrucomicrobiota. In the genus-level analysis results (Fig. 5E), the model group showed unusually high relative abundances of the potential pathogen *Desulfovibrio*, and beneficial bacteria such as *Akkermansia* and Lachnospiraceae_UCG-006. Conversely, the beneficial bacteria norank_f_*Eubacterium_coprostanoligenes*_group and *Candidatus_Saccharimonas* were markedly reduced. Following CA intervention, the abundances of beneficial bacteria groups, including norank_f_*Eubacterium_coprostanoligenes*_group and

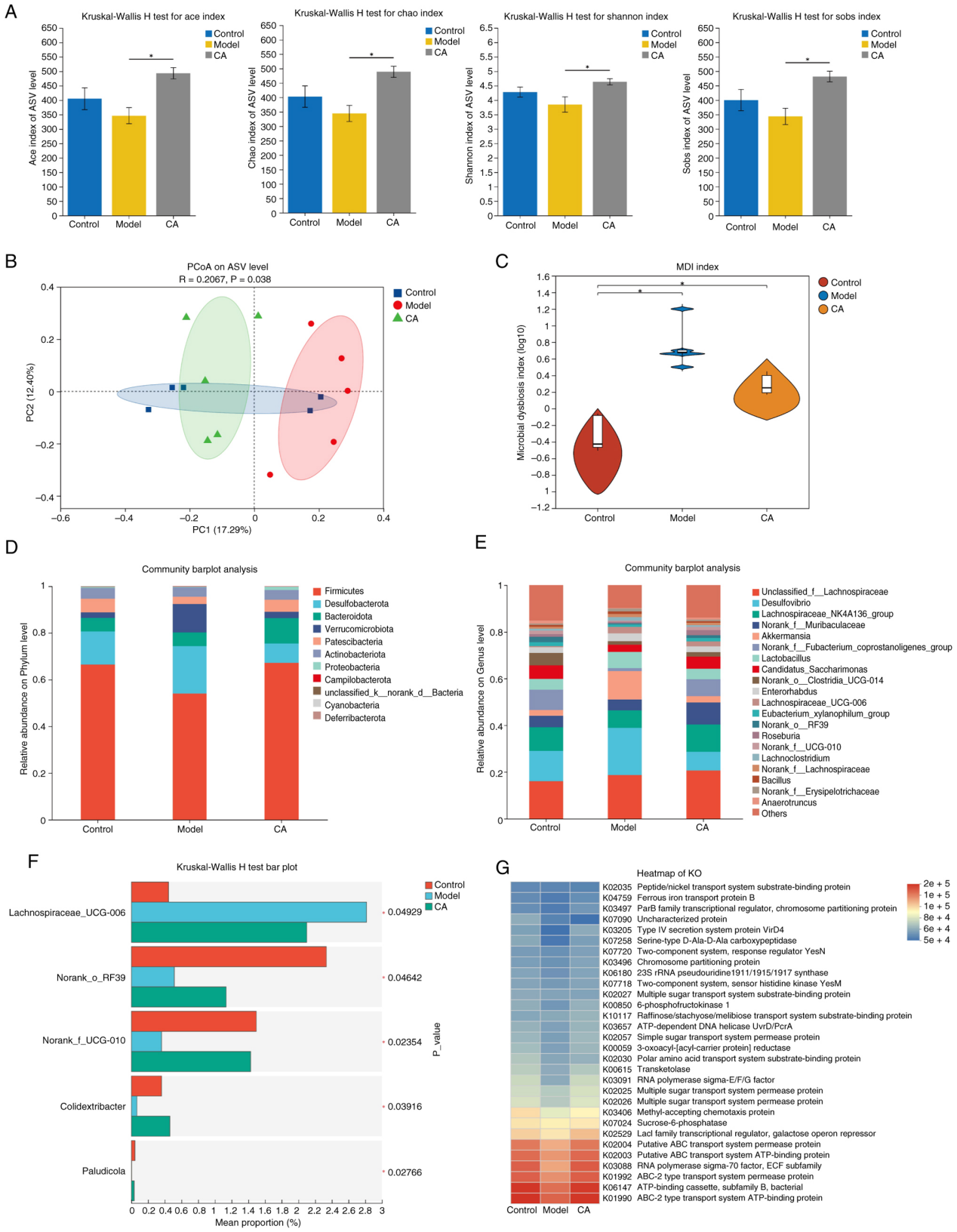

Figure 5. CA promotes gut microbiota diversity and modulates gut microbiota composition. (A) α-Diversity indices (ace, chao, shannon and sobs). (B) PCoA of β-diversity. (C) MDI index. (D) Gut microbiota composition at the phylum level. (E) Gut microbiota composition at the genus level. (F) Differentially abundant bacterial taxa identified by the Kruskal-Wallis H test. (G) PICRUSt2 Functional prediction heatmap. n=5. *P<0.05 vs. the model group. CA, 6'-O-Caffeoylarbutin; PCoA, principal co-ordinates analysis; MDI, microbiome dysbiosis index; PICRUSt2, Phylogenetic Investigation of Communities by Reconstruction of Unobserved States.

Candidatus_Saccharimonas, were markedly increased, whereas the abundance of the potential pathogen *Desulfovibrio* was decreased. Additionally, the normal levels of beneficial bacteria such as *Akkermansia* and Lachnospiraceae_UCG-006

were partly restored, indicating that CA aids in rebalancing the gut microbiota. Further statistical analysis of differential bacteria supported these findings (Fig. 5F), revealing that CA intervention markedly increased the abundances of norank_o_RF39, norank_f_UCG_010, *Colidextribacter* and *Paludicola*. Notably, the abundance of the beneficial bacterium *Lachnospiraceae*_UCG-006, which was abnormally elevated in the model group, showed a trend similar to the control group after CA intervention.

To further investigate the potential functional relevance of CA-associated gut microbiota remodeling, PICRUSt2-based functional prediction was performed using 16S rRNA sequencing data. As shown in Fig. 5G, the relative abundances of predicted KOs differed among the Control, Model, and CA groups. These differential KOs were mainly involved in membrane transport, substrate uptake, signal transduction, DNA replication/transcription-related processes and carbohydrate metabolism, including ABC transporter ATP-binding proteins, multiple sugar transport system permeases, substrate-binding proteins, two-component system regulators, ATP-dependent DNA helicase and RNA polymerase omega factors. Notably, several KOs that were altered in the Model group showed a trend toward restoration after CA treatment. These findings suggest that CA-associated microbial remodeling may be accompanied by shifts in the predicted functional potential of the gut microbiota.

Together, these findings suggested that HUA is associated with gut microbial dysbiosis, characterized by a reduction in beneficial taxa and an increase in potentially unfavorable microbial populations. CA treatment may partially ameliorate these alterations and reshape the gut microbial composition toward a healthier profile. These observations suggested that gut microbiota remodeling may be involved in the beneficial effects of CA in HUA model mice.

Discussion

Epidemiological evidence has indicated that ~90% of primary HUA cases arise from impaired UA excretion, rather than overproduction (11). CA, a natural compound isolated from traditional anti-gout herbal tea, may serve as a promising urate-lowering agent. Benzbromarone was included as a positive control in the present study, because it is a well-established uricosuric drug commonly used as a reference compound in experimental HUA models. Its primary pharmacological action involves promoting urate excretion through inhibition of renal urate reabsorption, particularly via URAT1-related pathways. In the present study, benzbromarone served as a benchmark for evaluating the anti-hyperuricemic efficacy of CA. Because the primary objective of the present study was to evaluate the therapeutic potential of CA and to preliminarily explore its underlying mechanisms, mechanistic analyses, including western blotting and gut microbiota profiling, were focused on the CA-treated groups rather than the positive control group. Therefore, benzbromarone was mainly used as a reference drug for comparison of anti-hyperuricemic efficacy and histopathological improvement. However, this study design limited direct mechanistic comparisons between benzbromarone and CA. In the current study, oral administration of CA markedly reduced SUA, SCr and BUN levels in HUA model mice, accompanied by histological protection in renal and intestinal tissues. Mechanistically, these urate-lowering effects were attributed to multiple coordinated actions: i) Modulation of aberrant urate transporter and scaffold protein expression (URAT1, GLUT9, ABCG2 and PDZK1) in the kidney and intestine; ii) upregulation of tight junction proteins (ZO-1, occludin and claudin-1), thereby restoring intestinal barrier integrity; and iii) preservation of gut microbial diversity, suppression of pathogenic taxa and re-establishment of microbial community homeostasis.

Regarding the regulation of urate transport, URAT1, GLUT9 and ABCG2 are recognized as major transporters involved in the gut-kidney axis of urate metabolism. Among these, renal urate handling primarily involves URAT1, GLUT9 and ABCG2, whereas intestinal urate excretion is more closely associated with GLUT9 and ABCG2 (42). Accordingly, the current study assessed URAT1, GLUT9 and ABCG2 in the kidney, and GLUT9, ABCG2 and PDZK1 in the intestine. This tissue-specific selection was based on their established roles in urate handling, with URAT1 predominantly mediating renal urate reabsorption, while intestinal urate transport mainly involves GLUT9 and ABCG2. PDZK1 was also included because it serves as an important scaffold protein that supports the apical localization and function of transporters such as ABCG2 in the intestinal epithelium (43).

URAT1, localized to the apical membrane of renal proximal tubular epithelial cells, is a key mediator of urate reabsorption, and its upregulation is closely associated with reduced urate excretion and elevated SUA levels (44,45). GLUT9 functions as a bidirectional urate transporter and cooperates with URAT1 in the regulation of urate reabsorption (46-48). ABCG2 is a key urate efflux transporter that mediates kidney and intestinal urate secretion. Dysfunction or reduced expression of ABCG2 impairs UA excretion, contributing to HUA and an increased risk of gout (49,50). For example, genetic deletion or pharmacological inhibition of ABCG2 has been shown to reduce intestinal UA clearance and induce compensatory renal excretion (51,52). The results of the present study showed that CA simultaneously improved the expression of urate transport-related proteins in both the kidney and intestine. Notably, these changes were functionally coordinated rather than mechanistically conflicting, providing further evidence that CA promotes urate excretion through a kidney-gut synergistic mechanism. In comparison to benzbromarone, the positive control used in the present study, CA may exhibit a potential advantage at the level of target regulation. Benzbromarone is primarily recognized as a uricosuric agent that lowers serum urate mainly through inhibition of renal urate reabsorption, particularly via URAT1-related pathways. By contrast, the present findings suggested that CA may exert a broader regulatory effect by simultaneously modulating urate transport-related proteins in both the kidney and intestine, indicating a more integrated mechanism for promoting urate excretion. This multi-target pattern may be beneficial for maintaining systemic urate homeostasis and could provide a broader translational potential than regulation restricted predominantly to the kidney.

As well as transporter regulation, the present study also highlighted the critical role of intestinal barrier integrity in the pathogenesis and treatment of HUA. The intestinal barrier consists of mechanical, chemical, immunological and

biological components, among which the mechanical barrier is a key factor in maintaining intestinal homeostasis. This barrier is primarily maintained by tight junction proteins (such as ZO-1, occludin and claudin-1), which prevent harmful luminal substances from entering the systemic circulation, thereby maintaining homeostasis (53). Previous studies have shown that under conditions of HUA, excessive UA and urate crystal deposition can damage intestinal epithelial cells and disrupt tight junction structures, leading to increased intestinal permeability (18,19). In the present study, CA markedly upregulated the expression levels of ZO-1, occludin and claudin-1 in intestinal tissue, while reducing serum levels of D-Lac, LPS, TNF-α and IL-6. These findings suggested that CA could improve intestinal barrier integrity and alleviate gut-derived inflammatory responses. Combined with the histopathological observations, the results further indicated that CA may reduce intestinal permeability by suppressing intestinal inflammation and restoring tight junction protein expression, thereby limiting endotoxin translocation and attenuating systemic chronic low-grade inflammation. This interpretation is consistent with the findings of a previous study showing that urate accumulation can impair intestinal barrier function and induce endotoxemia (19).

Notably, the present findings revealed organ-specific effects of CA on urate transporters. In the intestine, the 200 mg/kg dose produced slightly stronger effects than 300 mg/kg on ABCG2, PDZK1, GLUT9 and several tight junction proteins, whereas in the kidney the higher dose generally showed greater efficacy. This finding suggests that the effects of CA may not be strictly linear, but may vary across tissues and molecular endpoints. A possible explanation is that some intestinal targets respond optimally within a moderate dose range, whereas higher doses offer no additional benefit. This may be particularly relevant for epithelial transporters and barrier-related proteins, which are tightly regulated to maintain intestinal homeostasis and barrier integrity (53,54). In addition, as the intestine is the first site exposed to orally administered CA, differences in local exposure and mucosal metabolism may also contribute to the distinct intestinal and renal responses. In addition to regulating transporter expression, CA markedly affected the scaffold protein PDZK1, which may facilitate the apical localization and functional activity of transporters such as ABCG2, thereby promoting intestinal urate excretion. Overall, these findings support a coordinated kidney-gut mechanism underlying the urate-lowering effect of CA, although the basis for the apparent superiority of the intermediate dose in the intestine warrants further investigation.

Accumulating evidence has implicated gut microbiota dysbiosis as both a consequence and a driver of HUA (55). Previous studies have typically reported increased Firmicutes and decreased Bacteroidota abundances in HUA models, along with depletion of beneficial genera such as *Faecalibacterium*, *Bifidobacterium* and *Lactobacillus* (37,56,57). Notably, the current study identified a distinct microbial pattern characterized by reduced Firmicutes and increased Desulfobacterota and Verrucomicrobiota abundances, indicating a substantial disruption in microbial equilibrium. CA treatment effectively reversed these alterations, restoring phylum-level composition toward that of the control group mice. At the genus level, CA markedly increased the abundance of beneficial bacteria such as norank_f_*Eubacterium*_*coprostanoligenes*_group, *Candidatus*_*Saccharimonas*, *Colidextribacter, Paludicola* and norank_f_UCG-010. It was also observed that CA reduced the abundance of abnormally proliferating beneficial bacteria such as *Akkermansia* and *Lachnospiraceae*_UCG-006 to normal levels. Notably, elevated *Akkermansia* abundance has also been observed in patients with asymptomatic HUA (58), potentially reflecting a compensatory adaptation to microbial stress. Furthermore, the abundance of harmful bacteria, particularly *Desulfovibrio*, was markedly elevated in HUA model mice. *Desulfovibrio* is a gram-negative, sulfate-reducing anaerobe that generates hydrogen sulfide, a cytotoxic metabolite capable of impairing mitochondrial respiration, disrupting epithelial barriers and inducing inflammation (59). CA treatment markedly suppressed *Desulfovibrio* abundance, thereby stabilizing the intestinal microenvironment and mitigating inflammation. PICRUSt2-based functional prediction further suggested that HUA was accompanied by alterations in predicted microbial functions mainly related to transport systems, transcriptional regulation and general metabolic processes. Several differentially enriched KOs were associated with ABC transporters, sugar transport systems, transcriptional regulators and stress-response-related proteins, whereas CA treatment tended to shift these predicted functional profiles toward those of the control group. Although these findings require validation by metagenomic and metabolomic analyses, they support a potential association between CA-induced microbiota remodeling and the restoration of intestinal functional homeostasis. Collectively, these findings suggested that CA may exert beneficial effects on HUA, at least in part through modulation of gut microbiota composition and predicted microbial functions.

Recent studies have increasingly highlighted the critical role of the gut-kidney axis in the development and treatment of HUA. Zhou *et al* (60), Han *et al* (37) and Zhao *et al* (61) collectively demonstrated that modulation of the gut microbiota and improvement of renal-intestinal dysfunction are closely associated with alleviation of HUA and related renal injury. Overall, the present findings are consistent with these recent reports in supporting the hypothesis that restoration of gut microbial homeostasis and coordinated improvement of kidney-intestine function are important components of the anti-hyperuricemic effect. Notably, although the overall trend of microbiota normalization observed in the current study is in agreement with previous studies, the present study observed a specific phylum-level alteration pattern characterized by decreased Firmicutes and increased Bacteroidota in the model group. This discrepancy may be related to differences in experimental models, intervention compounds, treatment duration, or analytical conditions. Therefore, rather than indicating a contradiction, these findings suggested that different interventions may reshape the gut microbiota through partially distinct routes while ultimately converging on the common outcome of stabilizing microbial homeostasis and improving gut-kidney axis function in HUA.

Despite these promising findings, several limitations should be acknowledged. First, the current data are largely associative and do not establish causal relationships between the improvements in biochemical parameters and the observed changes in urate transporters, intestinal barrier integrity

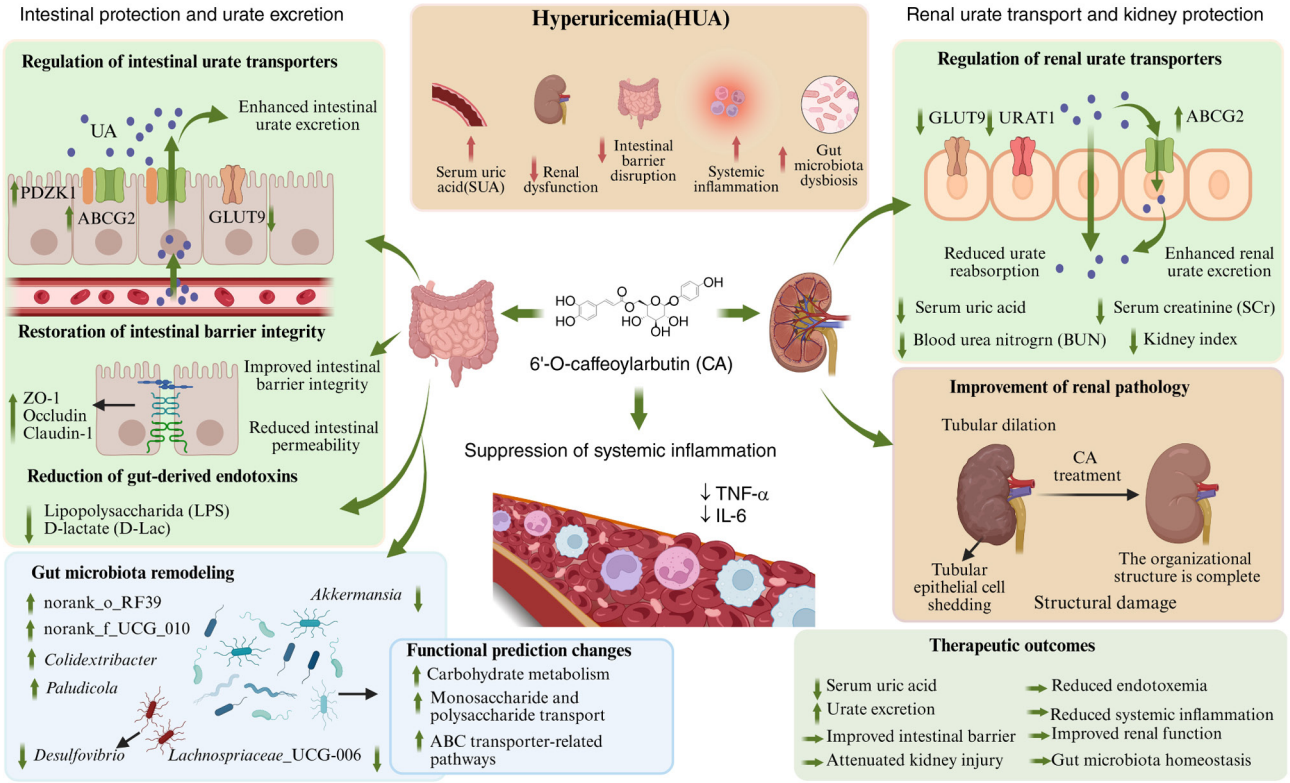

Figure 6. Schematic diagram illustrating the molecular mechanisms by which CA alleviates hyperuricemia. The compound reduces serum uric acid levels by regulating transporters in the kidney and intestine and protecting the intestinal barrier. (Created with BioRender.com). CA, 6'-O-Caffeoylarbutin; HUA, hyperuricemia; UA, uric acid; PDAZK1, PDZ domain containing 1; ABCG2, ATP-binding cassette sub-family G member 2; GLUT9, glucose transporter 9; ZO-1, zona occludens protein 1; URAT1, urate transporter 1; LPS, lipopolysaccharide; D-Lac, D-lactate; TNF-α, tumor necrosis factor-α; IL-6, interleukin-6; SUA, serum uric acid; SCr, serum creatinine; BUN, blood urea nitrogen.

and gut microbiota composition. Second, pharmacokinetic analyses, transporter functional assays, immunohistochemical validation and metabolomic profiling were not performed in the present study. Third, although gut microbiota remodeling was observed, causal experiments such as fecal microbiota transplantation or microbiota depletion were not conducted. Therefore, the precise molecular and microbial mechanisms underlying the effects of CA remain to be fully elucidated. Future studies integrating pharmacokinetic evaluation, multi-omics analyses and causality-based functional experiments will be essential to validate and extend the present findings.

In conclusion, a comprehensive working model for the anti-HUA mechanism of CA is proposed and presented in Fig. 6. Specifically, CA exerts potent urate-lowering and tissue-protective effects through the coordinated modulation of urate transporters, reinforcement of intestinal barrier integrity and restoration of gut microbial homeostasis. These findings highlight CA as a promising candidate compound for HUA therapy.

Acknowledgements

Not applicable.

Funding

The present study was supported by the First-Class Discipline Team of Kunming Medical University (grant no. 2024XKTDTS14) and the Kunming Medical University Postgraduate Innovation Fund Project (grant no. 2025S192).

Availability of data and materials

The data generated in the present study may be requested from the corresponding author.

Authors' contributions

BS and FL were responsible for writing, reviewing and editing the manuscript, writing the original draft, visualization (preparing the figures, tables and schematic diagrams), data analysis using appropriate analytical and visualization software, providing research materials, datasets and other resources required for the study, designing and implementing the research methodology, conducting the experiments and investigations, performing statistical analysis and interpretation of the data, data curation (organizing and extracting information from the relevant literature), project administration and conceptualization. XYu and YZ were responsible for supervision, data analysis using appropriate analytical software, designing and implementing the research methodology, conducting experiments and investigations, funding acquisition and conceptualization. KS, RY and XL were responsible for project administration, conducting experiments and investigations, and organizing and managing the collected data. XC, TL and XYa were responsible for validation (checking the accuracy and consistency of the experimental

results, extracted information, references and interpretations), data analysis using appropriate analytical and visualization software, providing research materials and other resources required for the study, and project administration. ML and LL were responsible for writing, reviewing and editing, supervision, designing and implementing the research methodology, funding acquisition and conceptualization. BS and FL confirm the authenticity of all the raw data. All authors read and approved the final manuscript.

Ethics approval and consent to participate

The present study adhered to ethical guidelines for animal research as per the approval of the Ethics Committee of Kunming Medical University (approval no. KMMU20240343).

Patient consent for publication

Not applicable.

Competing interests

The authors declare that they have no competing interests.

References

1. Maiuolo J, Oppedisano F, Gratteri S, Muscoli C and Mollace V: Regulation of uric acid metabolism and excretion. Int J Cardiol 213: 8-14, 2016.
2. Dehlin M, Jacobsson L and Roddy E: Global epidemiology of gout: Prevalence, incidence, treatment patterns and risk factors. Nat Rev Rheumatol 16: 380-390, 2020.
3. Klinenberg JR, Goldfinger SE and Seegmiller JE: The effectiveness of the xanthine oxidase inhibitor allopurinol in the treatment of gout. Ann Intern Med 62: 639-647, 1965.
4. Alotaibi T, Bjazevic J, Kim R, Gryn S, Sultan N, Dresser G and Razvi H: Allopurinol hypersensitivity syndrome Raising awareness of an uncommon but potentially serious adverse event among kidney stone patients. Can Urol Assoc J 18: E167-E172, 2024.
5. Wang M, Zhang Y, Zhang M, Li H, Wen C, Zhao T, Xie Z and Sun J: The major cardiovascular events of febuxostat versus allopurinol in treating gout or asymptomatic hyperuricemia: A systematic review and meta-analysis. Ann Palliat Med 10: 10327-10337, 2021.
6. No authors listed: Safety update: Febuxostat and CVD. Drug Ther Bull 61: 102, 2023.
7. Bai Y, Wu B, Gou L, Fang Z, Xu T, Zhang T and Li Y: Cardiovascular safety evaluation of febuxostat and allopurinol: Findings from the FDA adverse event reporting system. J Clin Med 12: 6089, 2023.
8. Mackenzie IS, Ford I, Nuki G, Hallas J, Hawkey CJ, Webster J, Ralston SH, Walters M, Robertson M, De Caterina R, *et al*: Long-term cardiovascular safety of febuxostat compared with allopurinol in patients with gout (FAST): A multicentre, prospective, randomised, open-label, non-inferiority trial. Lancet 396: 1745-1757, 2020.
9. van der Klauw MM, Houtman PM, Stricker BH and Spoelstra P: Hepatic injury caused by benzbromarone. J Hepatol 20: 376-379, 1994.
10. Ye X, Wu J, Tang K, Li W, Xiong C and Zhuo L: Benzbromarone as a possible cause of acute kidney injury in patients with urolithiasis: Two case reports. Medicine (Baltimore) 98: e15214, 2019.
11. Mehmood A, Zhao L, Ishaq M, Xin W, Zhao L, Wang C, Hossen I, Zhang H, Lian Y and Xu M: Anti-hyperuricemic potential of stevia (Stevia rebaudiana Bertoni) residue extract in hyperuricemic mice. Food Funct 11: 6387-6406, 2020.
12. Yanai H, Adachi H, Hakoshima M and Katsuyama H: Molecular biological and clinical understanding of the pathophysiology and treatments of hyperuricemia and its association with metabolic syndrome, cardiovascular diseases and chronic kidney disease. Int J Mol Sci 22: 9221, 2021.
13. Sorensen LB: Role of the intestinal tract in the elimination of uric acid. Arthritis Rheum 8: 694-706, 1965.
14. Adomako EA and Moe OW: Uric acid transport, transporters, and their pharmacological targeting. Acta Physiol (Oxf) 238: e13980, 2023.
15. Xu D, Lv Q, Wang X, Cui X, Zhao P, Yang X, Liu X, Yang W, Yang G, Wang G, *et al*: Hyperuricemia is associated with impaired intestinal permeability in mice. Am J Physiol Gastrointest Liver Physiol 317: G484-G492, 2019.
16. Li Y, Li H, Wang R, Yu Y, Liu X and Tian Z: Protective effect of sodium butyrate on intestinal barrier damage and uric acid reduction in hyperuricemia mice. Biomed Pharmacother 161: 114568, 2023.
17. Zhou Y, Zhao M, Pu Z, Xu G and Li X: Relationship between oxidative stress and inflammation in hyperuricemia: Analysis based on asymptomatic young patients with primary hyperuricemia. Medicine (Baltimore) 97: e13108, 2018.
18. Ma C, Yang X, Lv Q, Yan Z, Chen Z, Xu D, Liu X, Yang W and Xing S: Soluble uric acid induces inflammation via TLR4/NLRP3 pathway in intestinal epithelial cells. Iran J Basic Med Sci 23: 744-750, 2020.
19. Lv Q, Xu D, Ma J, Wang Y, Yang X, Zhao P, Ma L, Li Z, Yang W, Liu X, *et al*: Uric acid drives intestinal barrier dysfunction through TSPO-mediated NLRP3 inflammasome activation. Inflamm Res 70: 127-137, 2021.
20. Wei J, Zhang Y, Dalbeth N, Terkeltaub R, Yang T, Wang Y, Yang Z, Li J, Wu Z, Zeng C and Lei G: Association between gut microbiota and elevated serum urate in two independent cohorts. Arthritis Rheumatol 74: 682-691, 2022.
21. Wang Z, Li Y, Liao W, Huang J, Liu Y, Li Z and Tang J: Gut microbiota remodeling: A promising therapeutic strategy to confront hyperuricemia and gout. Front Cell Infect Microbiol 12: 935723, 2022.
22. Wang J, Chen Y, Zhong H, Chen F, Regenstein J, Hu X, Cai L and Feng F: The gut microbiota as a target to control hyperuricemia pathogenesis: Potential mechanisms and therapeutic strategies. Crit Rev Food Sci Nutr 62: 3979-3989, 2022.
23. Yin H, Liu N and Chen J: The role of the intestine in the development of hyperuricemia. Front Immunol 13: 845684, 2022.
24. Shi ZQ, Wen X, Wu XR, Peng HZ, Qian YL, Zhao YL and Luo XD: 6'-O-caffeoylarbutin of vaccinium dunalianum alleviated ischemic stroke through the PI3K/AKT/NF-κB pathway. Phytomedicine 139: 156505, 2025.
25. Wang Y, Wang Y, Zhao T, Zhou W, Khan A, Cao J, Liu Y, Wang Z and Cheng G: 6'-O-caffeoylarbutin attenuates D-galactose-induced brain and liver damage in aging mice via regulating SIRT1/NF-κB pathway. Phytomedicine 141: 156710, 2025.
26. Wang Y, Wang Z, Xue Q, Zhen L, Wang Y, Cao J, Liu Y, Khan A, Zhao T and Cheng G: Effect of ultra-high pressure pretreatment on the phenolic profiles, antioxidative activity and cytoprotective capacity of different phenolic fractions from Que Zui tea. Food Chem 409: 135271, 2023.
27. Wang YP, Wang YD, Liu YP, Cao JX, Yang ML, Wang YF, Khan A, Zhao TR and Cheng GG: 6'-O-Caffeoylarbutin from Que Zui tea ameliorates acetaminophen-induced liver injury via enhancing antioxidant ability and regulating the PI3K signaling pathway. Food Funct 13: 5299-5316, 2022.
28. Wang Y, Wang Y, Zhao T, Li M, Wang Y, Cao J, Liu Y, Wang Z and Cheng G: Protective effect of Que Zui Tea on d-galactose-induced oxidative stress damage in mice via regulating SIRT1/Nrf2 signaling pathway. Molecules 29: 1384, 2024.
29. Wu B, Li C, Kan H, Zhang Y, Rao X, Liu Y and Zhao P: Hypolipidemic and antithrombotic effect of 6'-O-caffeoylarbutin from vaccinium dunalianum based on zebrafish model, network pharmacology, and molecular docking. Molecules 29: 780, 2024.
30. Zhang JK, Zhou XL, Wang XQ, Zhang JX, Yang ML, Liu YP, Cao JX and Cheng GG: Que Zui tea ameliorates hepatic lipid accumulation and oxidative stress in high fat diet induced nonalcoholic fatty liver disease. Food Res Int 156: 111196, 2022.
31. Xu M, Lao QC, Zhao P, Zhu XY, Zhu HT, Luo XL, Yang CR, He JH, Li CQ and Zhang YJ: 6'-O-Caffeoylarbutin inhibits melanogenesis in zebrafish. Nat Prod Res 28: 932-934, 2014.
32. Zhou X, Zhang B, Zhao X, Lin Y, Wang J, Wang X, Hu N and Wang S: Chlorogenic acid supplementation ameliorates hyperuricemia, relieves renal inflammation, and modulates intestinal homeostasis. Food Funct 12: 5637-5649, 2021.
33. Lee SH, Kim KH, Lee SM, Park SJ, Lee S, Cha RH, Lee JW, Kim DK, Kim YS, Ye SK and Yang SH: STAT3 blockade ameliorates LPS-induced kidney injury through macrophage-driven inflammation. Cell Commun Signal 22: 476, 2024.

34. Bolyen E, Rideout JR, Dillon MR, Bokulich NA, Abnet CC, Al-Ghalith GA, Alexander H, Alm EJ, Arumugam M, Asnicar F, *et al*: Reproducible, interactive, scalable and extensible microbiome data science using QIIME 2. Nat Biotechnol 37: 852-857, 2019.
35. Schloss PD, Westcott SL, Ryabin T, Hall JR, Hartmann M, Hollister EB, Lesniewski RA, Oakley BB, Parks DH, Robinson CJ, *et al*: Introducing mothur: open-source, platform-independent, community-supported software for describing and comparing microbial communities. Appl Environ Microbiol 75: 7537-7541, 2009.
36. Liu C, Ruan F, Chen Z, Han J, Ding X, Han C, Ye L, Yang C, Yu Y, Zuo Z and He C: Phenanthrene-induced hyperuricemia with intestinal barrier damage and the protective role of theabrownin: Modulation by gut microbiota-mediated bile acid metabolism. Sci Total Environ 949: 174923, 2024.
37. Han QQ, Ren QD, Guo X, Farag MA, Zhang YH, Zhang MQ, Chen YY, Sun ST, Sun JY, Li NY and Liu C: Punicalagin attenuates hyperuricemia via restoring hyperuricemia-induced renal and intestinal dysfunctions. J Adv Res 69: 449-461, 2025.
38. Guo LF, Chen X, Lei SS, Li B, Zhang NY, Ge HZ, Yang K, Lv GY and Chen SH: Effects and mechanisms of Dendrobium officinalis six nostrum for treatment of hyperuricemia with hyperlipidemia. Evid Based Complement Alternat Med 2020: 2914019, 2020.
39. Pickard JM, Zeng MY, Caruso R and Núñez G: Gut microbiota: Role in pathogen colonization, immune responses, and inflammatory disease. Immunol Rev 279: 70-89, 2017.
40. Fan Y and Pedersen O: Gut microbiota in human metabolic health and disease. Nat Rev Microbiol 19: 55-71, 2021.
41. Chen Y, Zhou J and Wang L: Role and mechanism of gut microbiota in human disease. Front Cell Infect Microbiol 11: 625913, 2021.
42. Kim SH, Shin J, Son HE and Kang DH: Role of urate transporters in the kidneys and intestine in uric acid homeostasis. Kidney Res Clin Pract 45: 296-313, 2026.
43. Xu YX, Liu LD, Zhu JY, Zhu SS, Ye BQ, Yang JL, Huang JY, Huang ZH, You Y, Li WK, *et al*: Alistipes indistinctus-derived hippuric acid promotes intestinal urate excretion to alleviate hyperuricemia. Cell Host Microbe 32: 366-381.e9, 2024.
44. Cho SK, Kim S, Chung JY and Jee SH: Discovery of URAT1 SNPs and association between serum uric acid levels and URAT1. BMJ Open 5: e009360, 2015.
45. Dai Y and Lee CH: Transport mechanism and structural pharmacology of human urate transporter URAT1. Cell Res 34: 776-787, 2024.
46. Shen Z, Xu L, Wu T, Wang H, Wang Q, Ge X, Kong F, Huang G and Pan X: Structural basis for urate recognition and apigenin inhibition of human GLUT9. Nat Commun 15: 5039, 2024.
47. Auberson M, Stadelmann S, Stoudmann C, Seuwen K, Koesters R, Thorens B and Bonny O: SLC2A9 (GLUT9) mediates urate reabsorption in the mouse kidney. Pflugers Arch 470: 1739-1751, 2018.
48. Ruiz A, Gautschi I, Schild L and Bonny O: Human mutations in SLC2A9 (Glut9) affect transport capacity for urate. Front Physiol 9: 476, 2018.
49. Matsuo H, Takada T, Nakayama A, Shimizu T, Sakiyama M, Shimizu S, Chiba T, Nakashima H, Nakamura T, Takada Y, *et al*: ABCG2 dysfunction increases the risk of renal overload hyperuricemia. Nucleosides Nucleotides Nucleic Acids 33: 266-274, 2014.
50. Hoque KM, Dixon EE, Lewis RM, Allan J, Gamble GD, Phipps-Green AJ, Halperin Kuhns VL, Horne AM, Stamp LK, Merriman TR, *et al*: The ABCG2 Q141K hyperuricemia and gout associated variant illuminates the physiology of human urate excretion. Nat Commun 11: 2767, 2020.
51. Ichida K, Matsuo H, Takada T, Nakayama A, Murakami K, Shimizu T, Yamanashi Y, Kasuga H, Nakashima H, Nakamura T, *et al*: Decreased extra-renal urate excretion is a common cause of hyperuricemia. Nat Commun 3: 764, 2012.
52. Hosomi A, Nakanishi T, Fujita T and Tamai I: Extra-renal elimination of uric acid via intestinal efflux transporter BCRP/ABCG2. PLoS One 7: e30456, 2012.
53. Chelakkot C, Ghim J and Ryu SH: Mechanisms regulating intestinal barrier integrity and its pathological implications. Exp Mol Med 50: 1-9, 2018.
54. Turner JR: Intestinal mucosal barrier function in health and disease. Nat Rev Immunol 9: 799-809, 2009.
55. Singh AK, Durairajan SSK, Iyaswamy A and Williams LL: Elucidating the role of gut microbiota dysbiosis in hyperuricemia and gout: Insights and therapeutic strategies. World J Gastroenterol 30: 4404-4410, 2024.
56. Chen Q, Li D, Wu F, He X, Zhou Y, Sun C, Wang H and Liu Y: Berberine regulates the metabolism of uric acid and modulates intestinal flora in hyperuricemia rats model. Comb Chem High Throughput Screen 26: 2057-2066, 2023.
57. Guo Y, Yu Y, Li H, Ding X, Li X, Jing X, Chen J, Liu G, Lin Y, Jiang C, *et al*: Inulin supplementation ameliorates hyperuricemia and modulates gut microbiota in Uox-knockout mice. Eur J Nutr 60: 2217-2230, 2021.
58. Yang HT, Xiu WJ, Liu JK, Yang Y, Hou XG, Zheng YY, Wu TT, Wu CX and Xie X: Gut Microbiota characterization in patients with asymptomatic hyperuricemia: Probiotics increased. Bioengineered 12: 7263-7275, 2021.
59. Xie R, Gu Y, Li M, Li L, Yang Y, Sun Y, Zhou B, Liu T, Wang S, Liu W, *et al*: *Desulfovibrio* vulgaris interacts with novel gut epithelial immune receptor LRRC19 and exacerbates colitis. Microbiome 12: 4, 2024.
60. Zhou X, Ji S, Chen L, Liu X, Deng Y, You Y, Wang M, He Q, Peng B, Yang Y, *et al*: Gut microbiota dysbiosis in hyperuricaemia promotes renal injury through the activation of NLRP3 inflammasome. Microbiome 12: 109, 2024.
61. Zhao Y, Wang R, Cao R, Chen L, Chen L and Teng H: Galangin protects against hyperuricemia via ameliorating gut-kidney axis dysfunction in mice. J Agric Food Chem 73: 13902-13917, 2025.